

Interferometric measurement of Van Hove singularities in strained graphene

Samad Roshan Entezar
University of Tabriz, Tabriz, Iran
s-roshan@tabrizu.ac.ir

January 5, 2022

Abstract

This study presents a method based on the total internal reflection and the phase-shifting interferometry for measuring the Van Hove singularities in strained graphene. A linearly polarized light passes through some quarter- and half-wave plates, a hemi-cylindrical prism, and a Mach-Zehnder interferometer. The Van Hove singularities manifest themselves as some sharp dips or peaks in the spectrum of the final phase difference of the two interference signals. The numerical analysis demonstrates that the number of Van Hove singularities is independent of the modulus of the applied stress, but their position shifts as the strength of the tension increases. Besides, the number and location of singularities strongly depend on the stress direction relative to the zigzag axis in the graphene lattice. Moreover, we show that the location of singularities is independent of the tension direction relative to the tangential component of the electric field of the incident radiation.

keywords: Graphene, strain, phase-shifting interferometry, total internal reflection.

1 Introduction

Graphene as a single sheet of carbon atoms in a hexagonal lattice has shown abundant new physics and potential applications in carbon-based nanoelectronic devices because of its exceptional electrical and optical properties [1–5].

It has the highest known electrical and thermal conductivity, as well as the highest stiffness and strength [6]. The ability to modify the electronic structure of graphene is needed to make a graphene-based device or circuit. Possible tools for achieving this goal include patterning, electric field effects, and chemical doping [7–9]. Recently, it has even been proposed that strain can be used to achieve various essential elements for all-graphene electronics [10]. The strain effect in graphene provides a new way to manipulate electron transport without external fields. Graphene is structurally more tolerant than silicon to external effects such as strain. Graphene, as the strongest material ever measured, can also support strain well beyond the linear regime, without to be bent or wrinkled. Very high strains can be easily exerted on graphene before the mechanical failure [11–15]. The effect of strain on graphene has been studied both experimentally and theoretically [16–20]. The mechanical strain often has unexpected effects on the electronic properties of carbon nanomaterials [21–27]. Graphene offers a new opportunity to discover such interesting electromechanical properties in two dimensions [7]. Mechanically strained graphene may introduce a new environment to study the novel physical phenomena [28–30]. The strain may be applied naturally or intentionally to graphene.

In many applications, graphene lays or grows on a substrate. Growth of graphene on substrates like SiO₂ or SiC with a different lattice constant usually introduces strain due to surface corrugations or lattice mismatch [31, 32], which can be detected by Raman spectroscopy [33]. Even in the absence of a mismatch, the strain still occurs along the edges and exhibits some interesting quantum properties [34, 35]. Bending the substrates may induce a uniaxial strain on it [12–14, 36]. Using tension to control the physical properties of graphene has attracted an ever-increasing interest [37–46].

From a technological point of view, understanding how strain affects graphene’s electronic and optical properties is of paramount importance. Since the electronic states near the Fermi level are directly related to optical and transport properties of graphene, most researchers have focused on the electronic structure of graphene near the Dirac points [47–54]. Moreover, the density state may exhibit one or more Van Hove singularities. The wavevectors at which Van Hove singularities occur are often referred to as critical points of the Brillouin zone [55]. In bulk solids, the presence of Van Hove singularities in the density of states will result in strong optical absorption peaks as well as Raman signals. However, in graphene systems, few empirical studies show the existence of Van Hove singularities [56, 57]. The

existence of Van Hove singularities in graphene structures may be influenced by strain [58]. Motivated by this, we want to investigate Van Hove singularities in strained graphene. In this paper, we present a method for measuring the frequency of Van Hove singularities, based on Fresnel equations [59] and the phase-shifting interferometry [60]. A linearly polarized light beam passes through a phase-sensitive internal reflection device, consisting of a hemicylindrical prism, two half-wave plates, and two quarter-wave with proper azimuth angles. The output beam enters a Mach-Zehnder interferometer with two acousto-optic modulators separately placed in two arms. Eventually, the two linearly orthogonal polarizations of each output beam of the interferometer interfere with each other as they pass through two analyzers, respectively. The ultimate phase difference between the two interference signals is associated with the azimuth angle of the fast axis of the half-wave plates, yielding the sensitivity-tunable functionality.

1.1 Theoretical calculation and model

Let us consider a single flat sheet of mono-layer graphene deposited on a substrate of refractive index n_s , which is capped by a high-index prism of refractive index n_p . A laser beam is incident upon the base of the prism at the angle of incidence ϑ (see Fig. 1(a)). The reflection and transmission coefficients of the structure are determined by satisfying the continuity of the tangential component of the electric fields and the discontinuity of the tangential component of the magnetic fields caused by the induced surface

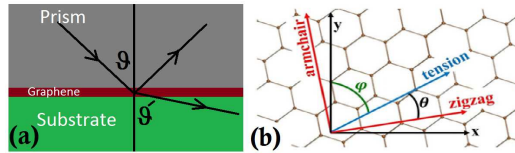


Figure 1: a) The geometry of the problem with monolayer graphene deposited on a substrate. Light is incident from a high-index prism at the incidence angle ϑ . b) The graphene honeycomb lattice with its zigzag and armchair directions, and the tension direction. Here, θ and φ denote the angles which the applied strain makes with the zigzag path and the tangential electric field, respectively.

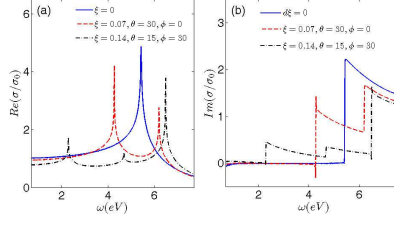


Figure 2: a) The real and b) the imaginary parts of the normalized optical conductivity of the strained graphene versus photon energy ω .

current in graphene as

$$\begin{aligned}
 r_s &= \frac{n_p \cos \vartheta - n_s \cos \vartheta' - \eta_0 \sigma}{n_p \cos \vartheta + n_s \cos \vartheta' + \eta_0 \sigma}, \\
 r_p &= \frac{n_s \cos \vartheta - n_p \cos \vartheta' + \eta_0 \sigma \cos \vartheta \cos \vartheta'}{n_s \cos \vartheta + n_p \cos \vartheta' + \eta_0 \sigma \cos \vartheta \cos \vartheta'},
 \end{aligned} \tag{1}$$

$$\begin{aligned}
 t_s &= \frac{2n_p \cos \vartheta n_p \cos \vartheta + n_s \cos \vartheta' + \eta_0 \sigma}{2n_s \cos \vartheta}, \\
 t_p &= \frac{2n_s \cos \vartheta}{n_s \cos \vartheta + n_p \cos \vartheta' + \eta_0 \sigma \cos \vartheta \cos \vartheta'}.
 \end{aligned} \tag{2}$$

Here, η_0 is the intrinsic impedance of free space, and σ is the optical conductivity of graphene monolayer. As one knows, the optical conductivity of the graphene is the sum of the intraband conductivity (due to the intraband electron-photon scattering processes) and the interband conductivity (which originates from the direct interband electron transitions) [61]. The optical conductivity of the graphene has been derived using perturbation theory in references [62, 63]. It was shown that the applied tension deforms the graphene lattice and distorts the reciprocal lattice [64]. Since the conduction and valence energy bands of the graphene vary due to the lattice deformation, the induced tension changes the optical conductivity of graphene [64]. We use the procedure explained in [61–64] to obtain σ under the applied tension without giving its explicit form here. Figure 2 shows a) the real and b) the imaginary parts of σ (in the unite of $\sigma_0 = \frac{e^2}{4h}$) versus the photon energy (ω) for applied tension with different modules at different directions. Here, we assume that the direction of the applied tension makes angles θ

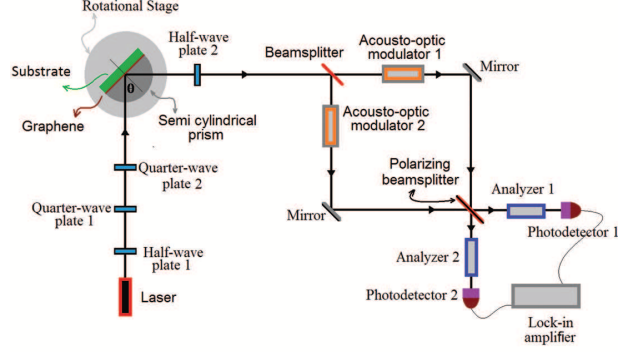


Figure 3: Schematic diagram for measuring the phase difference ψ .

and φ with the zigzag path in the graphene honeycomb lattice and the tangential electric field of the incident beam respectively, and ζ indicates the strain modulus (see Fig. 1(b)). We see some maxima at the real part of σ which, are attributed to the Van Hove singularities at the saddle-points of the electronic band structure of the graphene in the UV band [58, 64, 65]. In unstrained graphene, there are three equivalent saddle-points in the electronic band structure, which show themselves as a single peak in the optical conductivity (see dotted lines in Fig. 2). In the strained graphene, at most two of the saddle-points may be equivalent. As a result, we see two or three peaks in σ . The number of peaks and their position strongly depend on the modulus and direction of the applied tension.

Here, we would like to present a simple procedure to obtain the effect of applied tension on the position of the Van Hove singularities. The schematic experimental setup for this measurement is shown in Fig. 3. For convenience, we consider the direction of the propagated light beam as the z -axis and set the x -axis perpendicular to the plane of the paper. A linear s -polarized laser light after passing through the half-wave plate 1 (with the fast axis at $\Delta/2$ with respect to the x -axis), the quarter-wave plate 1 (with the slow axes at 45° with respect to the x -axis) and the quarter-wave plate 2 (with its slow axes along the x -axis) is incident vertically on a hemi-cylindrical prism with the refractive index of n_p . The light ray is refracted into the prism, and it propagates at the incidence angle ϑ toward the boundary surface between the prism and the graphene monolayer. For ϑ larger than the critical angle $\sin^{-1} \frac{n_s}{n_p}$, the light undergoes total internal reflection at the boundary. Then the reflected light beam travels through the half-wave plate 2, which its fast

axes makes angle α with the x-axis. The Jones vector of the light after the half-wave plate 2 can be written as:

$$\begin{aligned} E_t &= \begin{pmatrix} A_s e^{i\phi_s} \\ A_p e^{i\phi_p} \end{pmatrix} \\ &= \frac{t\acute{t}}{\sqrt{2}} \begin{pmatrix} r_s \cos 2\alpha e^{-i\Delta} + r_p \sin 2\alpha e^{-i\Delta} \\ r_s \sin 2\alpha e^{-i\Delta} - r_p \cos 2\alpha e^{-i\Delta} \end{pmatrix}, \end{aligned} \quad (3)$$

where

$$t = \frac{2}{n_p + 1}, \quad \acute{t} = \frac{2n_p}{n_p + 1}, \quad (4)$$

Here, t , \acute{t} are the transmission coefficients at the air-prism and the prism-air interface, respectively. A 50/50 beam splitter of a Mach-Zehnder interferometer splits the reflected light beam into reflected and transmitted beams after passing through the half-wave plate 2. Those beams pass through the electro-optical modulators 1 and 2 to shift their frequencies to ω_1 and ω_2 , respectively. Then, a polarizing beam splitter superimposes the beams. The output beams after passing through the analyzers 1 and 2 (which their transmission axis makes angle β with the x-axis) are detected using the photo-detectors 1 and 2 in both output ports. The intensities measured by the photo-detectors 1 and 2 are

$$\begin{aligned} I_1 &= \frac{1}{2}(A_s^2 \cos^2 \beta + A_p^2 \sin^2 \beta \\ &+ \sin 2\beta A_s A_p \cos[(\omega_2 - \omega_1)t + (\phi_p - \phi_s)]), \end{aligned} \quad (5)$$

$$\begin{aligned} I_2 &= \frac{1}{2}(A_s^2 \cos^2 \beta + A_p^2 \sin^2 \beta \\ &+ \sin 2\beta A_s A_p \cos[(\omega_2 - \omega_1)t - (\phi_p - \phi_s)]). \end{aligned} \quad (6)$$

The intensities I_1 and I_2 , are sent to a lock-in amplifier to obtain the phase difference $\psi = 2(\phi_p - \phi_s)$.

2 Results and numerical calculations

In this section we describe the numerical analysis. Here, we assumed that the incidence angle ϑ to be $\approx 52.2^\circ$, $n_p = 1.7786$, $n_s = 1.4$, $\alpha \cong 25^\circ$, $\Delta \approx 25^\circ$

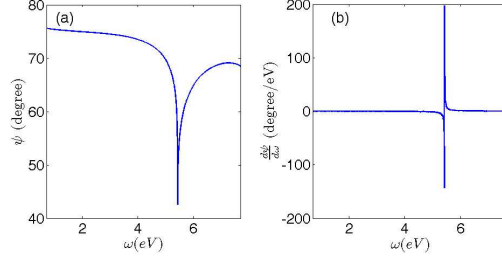


Figure 4: a) Phase difference ψ and b) the sensitivity $\frac{d\psi}{d\omega}$ vs photon energy (ω) in the absence of the strain.

and $\beta \approx 0^\circ$, respectively. Fig. 4 depicts the simulated results by plotting a) the phase difference ψ and b) the sensitivity $\frac{d\psi}{d\omega}$ vs photon energy (ω) in the absence of the strain. As it is clear from Fig. 4(a), the phase difference ψ monotonically decreases to reach its minimum at a specific frequency and then increases by increasing ω . We find that the phase difference changes its behavior at the frequency in which the Van Hove singularity occurred (compare Figs. 4(a) and 2(a) (the dotted-dashed line)). In this method, the Van Hove singularity exhibit itself as a sharp peak or deep valley in the phase difference curve. From Fig. 4(b), we find that this method has an acceptable sensitivity ($\frac{d\psi}{d\omega}$) to obtain the frequencies at which the Van Hove singularities occur. Now we consider the phase difference curve for the case

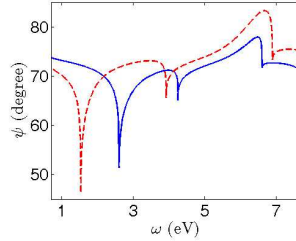


Figure 5: The phase difference ψ vs the photon energy (ω) for two different moduli $\zeta = 0.14$ (the solid line) and $\zeta = 0.21$ (the dashed line) of the applied strain with the fixed direction at $\theta = 20^\circ$, and $\varphi = 0$.

of strained graphene. We first study the case of graphene under strain in a given direction with different moduli of applied strain. Figure 5 shows the phase difference ψ vs the photon energy (ω) for two different moduli $\zeta = 0.14$

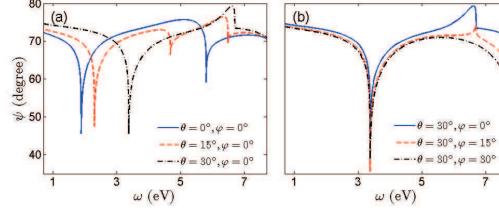


Figure 6: The phase difference ψ vs the photon energy (ω) for three different directions of the applied strain at a) $\theta = 0^\circ$, (the solid line), $\theta = 15^\circ$, (the dashed line), $\theta = 30^\circ$ with $\varphi = 0$ (the dotted-dash line) and b) $\varphi = 0^\circ$ (the solid line), $\varphi = 15^\circ$, $\varphi = 30^\circ$ (the dashed line) with $\theta = 30^\circ$. Here, the modulus of the applied strain (ζ) is 0.14.

(the solid line) and $\zeta = 0.21$ (the dashed line) of the applied strain with the fixed direction of the applied strain at $\theta = 20^\circ$ and $\varphi = 0$. From the figure, we see that the number of sharp deeps in the phase difference curve has increased to three due to the stress, which indicates the existence of three Van Hove singularities in the density of states of the strained graphene. It is clear from the figure that the position of the singularities changes slightly as the stress increases. The first two singularities move to lower frequencies, and the third singularity suffers from a blue-shift. We also note that the number of Van Hove singularities is independent of the modulus of applied stress.

Finally, we consider the phase difference curve for the case of strained graphene at different directions of the applied strain with a given modulus. Figure 6 depicts the phase difference ψ vs the photon energy (ω) for three different directions of the applied strain at a) $\theta = 0^\circ$, (the solid line), $\theta = 15^\circ$, (the dashed line), $\theta = 30^\circ$ (the dotted-dash line) with $\varphi = 0$ and b) $\varphi = 0^\circ$ (the solid line), $\varphi = 15^\circ$, $\varphi = 30^\circ$ (the dashed line) with $\theta = 30^\circ$. Here, we considered the modulus of the applied strain (ζ) to be 0.14. As one knows, θ is the angle between the direction of the applied tension and the zigzag path in the graphene honeycomb lattice, and φ indicates the angle between the directions of the applied tension and the tangential electric field of the incident beam. Figure 6 reveals that the number of the Van Hove singularities strongly depends on both θ and φ , and it varies from one to three. However, the frequency location of the Van Hove singularities depends solely on θ and it is independent of φ .

3 Conclusions

An experimental method for measuring the frequency of the Van Hove singularities in the density of states of strained graphene is proposed. The phase difference of p- and s-polarized reflected light under the total internal reflection in a hemi-cylindrical prism, whose base is contacted with the strained graphene, can be measured accurately with the phase-shifting interferometry. The Van Hove singularities present themselves as some sharp dips or peaks in the phase difference spectrum. The validity of the method has been examined using the special equations derived to estimate the phase difference of the interferometric signals. We showed that the number of Van Hove singularities strongly depends on the direction of the applied strain. Not only the direction of the applied strain but also its modulus affects the frequency locations of the Van Hove singularities. We demonstrated the phase-shifting interferometry has an acceptable sensitivity to obtain the frequency of the Van Hove singularities.

References

- [1] Novoselov, K.S.; Geim, A.K.; Morozov, S.V. Jiang, D.; Zhang, Y.; Dubonos, S.V.; Grigorieva, I.V.; Firsov, A.A. Report electric field effect in atomically thin carbon films. *Science* 2004, 306, 666-669.
- [2] Zhang, Y.; Tan, Y.W.; Stormer, H.L.; Kim, P. Experimental observation of the quantum Hall effect and Berry's phase in graphene. *Nature* (London) 2005, 438, 201-204.
- [3] Geim, A. K.; Novoselov, K.S.; The rise of graphene. *Nat. Mater.* 2007, 6, 183-191.
- [4] Cresti, A.; Nemec, N.; Biel, B.; Niebler, G.; Triozon, F.; Cuniberti, G.; Roche, S. Charge transport in disordered graphene-based low dimensional materials. *Nano Res.* 2008, 1, 361-394.
- [5] Castro Neto; A.H., Guinea, F.; Peres, N.M.R.; Novoselov, K.S.A.; Geim, K. The electronic properties of graphene. *Rev. Mod. Phys.* 2009, 81, 109-162.

- [6] Balandin, A.A.; Ghosh, S.; Bao, W.; Calizo, I.; Teweldebrhan, D.; Miao, F.; Lau, C.N. Superior thermal conductivity of single-layer graphene. *Nano Lett.* 2008, 8 902-907
- [7] Novoselov, K.S.; Geim, A.K.; Morozov, S.V.; Jiang, D.; Zhang, Y.; Dubonos, S.V. Grigorieva, I.V.; Firsov, A.A. Electric field effect in atomically thin carbon films. *Science* 2004, 306, 666-669.
- [8] Yan, Q.M.; Huang, B.; Yu, J.; Zheng, F.W.; Zang, J.; Wu, J.; Gu, B.L.; Liu, F.; Duan, W.H. Intrinsic current-voltage characteristics of graphene nanoribbon transistors and effect of edge doping. *Nano Lett.* 2007, 7, 1469-1473.
- [9] Biel, B.; Blase, X.; Triozon, F.; Roche, S. Anomalous doping effects on charge transport in graphene nanoribbons. *Phys. Rev. Lett.* 2009, 102, 096803.
- [10] Pereira, V.M.; Neto, A.H.C. Strain engineering of graphene's electronic structure. *Phys. Rev. Lett.* 2009, 103, 046801.
- [11] Lee, C.; Wei, X.D.; Kysar, J.W.; Hone, J. Measurement of the elastic properties and intrinsic strength of monolayer graphene. *Science* 2008, 321, 385-388.
- [12] Ni, Z.H.; Yu, T.; Lu, Y.H.; Wang, Y.Y.; Feng, Y.P.; Shen, Z.X. Uniaxial strain on graphene: Raman spectroscopy study and band-gap opening. *ACS Nano* 2008, 2, 2301-2305.
- [13] Mohiuddin, T.M.G.; Lombardo, A.; Nair, R.R.; Bonetti, A.; Savini, G.; Jalil, R.; Bonini, N.; Basko, D. M.; Galiotis, C.; Marzari, N.; Novoselov, K.S.; Geim, A.K.; Ferrai, A.C. Uniaxial strain in graphene by Raman spectroscopy: G peak splitting, Gruneisen parameters, and sample orientation. *Phys. Rev. B* 2009, 79, 205433.
- [14] Kim, K.S.; Zhao, Y.; Jang, H.; Lee, S.Y.; Kim, J.M.; Kim, K.S.; Ahn, J.-H.; Kim, P.; Choi, J.-Y.; Hong, B.H. Large-scale pattern growth of graphene films for stretchable transparent electrodes. *Nature* 2009, 457, 706-710.

- [15] Bao, W.Z.; Miao, F.; Chen, Z.; Zhang, H.; Jang, W.Y.; Dames, C.; Lau, C.N. Controlled ripple texturing of suspended graphene and ultrathin graphite membranes. *Nat. Nanotechnol.* 2009, 4, 562-566.
- [16] Gui, G.; Li, J.; Zhong, J.X. Band structure engineering of graphene by strain: First-principles calculations. *Phys. Rev. B* 2008, 78, 075435.
- [17] Pereira, V.M.; Castro Neto, A.H.; Peres, N.M.R. Tightbinding approach to uniaxial strain in graphene. *Phys. Rev. B* 2009, 80, 045401.
- [18] Farjam, M.; Rafii-Tabar, H. Comment on "Band structure engineering of graphene by strain: First-principles calculations". *Phys. Rev. B* 2009, 80, 167401.
- [19] Gui, G.; Li, J.; Zhong, J.X. Reply to "Comment on 'Band structure engineering of graphene by strain: First-principles calculations'". *Phys. Rev. B* 2009, 80, 167402.
- [20] Guinea, F.; Katsnelson, M.I.; Geim, A.K. Energy gaps and a zero-field quantum Hall effect in graphene by strain engineering. *Nat. Phys.* 2009, 6, 30-33.
- [21] Heyd, R.; Charlier, A.; McRae, E. Uniaxial-stress effects on the electronic properties of carbon nanotubes. *Phys. Rev. B* 1997, 55, 6820-9824.
- [22] Yang, L.; Anantrun, M.P.; Han, J.; Lu, J.P. Band-gap change of carbon nanotubes: Effect of small uniaxial and torsional strain. *Phys. Rev. B* 1999, 60, 13874-13878.
- [23] Tombler, T.W.; Zhou, C.; Alexseyev, L.; Kong, J.; Dai, H.; Liu, L.; Jayanthi, C.S.; Tang, M.; Wu, S.Y. Reversible electromechanical characteristics of carbon nanotubes under local-probe manipulation. *Nature (London)* 2000, 405, 769-772.
- [24] Yang, L.; Han, J. Electronic Structure of Deformed Carbon Nanotubes. *Phys. Rev. Lett.* 2000, 85, 154-157.
- [25] Yu, M.-F.; Lourie, O.; Dyer, M.J.; Moloni, K.; Kelly, T.F.; Ruoff, R. Strength and breaking mechanism of multiwalled carbon nanotubes under tensile load. *Science* 2000, 287, 637-640.

- [26] Minot, E.D.; Yaish, Y.; Sazonova, V.; Park, J.; Brink, M.; McEuen, P.L. Tuning Carbon Nanotube Band Gaps with Strain. *Phys. Rev. Lett.* 2003, 90, 156401.
- [27] Sazonova, V.; Yaish, Y.; Ustunel, H.; Roundy, D.; Arias, T.A.; McEuen, P.L. A tunable carbon nanotube electrochemical oscillator. *Nature (London)* 2004, 431, 284-287.
- [28] Novoselov, K.S.; Geim, A.K.; Morozov, S.V.; Jiang, D.; Katsnelson, M.I.; Grigorieva, I.V.; Dubonos, S.V.; Firsov, A.A. Two-dimensional gas of massless Dirac fermions in graphene. *Nature (London)* 2005, 438, 197-200.
- [29] Park, C.-H.; Son, Y.W.; Yang, L.; Cohen, M.L.; Louie, S.G. Electron beam supercollimation in graphene superlattices. *Nano Lett.* 2008, 8, 2920-2924.
- [30] Park, C.-H.; Yang, L.; Son, Y.-W.; Cohen, M.L.; Louie, S.G. New Generation of Massless Dirac Fermions in Graphene under External Periodic Potentials. *Phys. Rev. Lett.* 2008, 101, 126804.
- [31] Ferralis, N.; Maboudian, R.; Carraro, C. Evidence of structural strain in epitaxial graphene layers on 6H-SiC(0001). *Phys. Rev. Lett.* 2008, 101, 156801.
- [32] Teague, M.L.; Lai, A.P.; Velasco, J.; Hughes, C.R.; Beyer, A.D.; Bockrath, M.W.; Lau, C.N.; Yeh, N.C. Evidence for Strain-Induced Local Conductance Modulations in Single-Layer Graphene on *SiO*₂. *Nano Lett.* 2009, 9, 2542-2546.
- [33] Borysiuk, J.; Bozek, R.; Strupinski, W.; Wyszomolek, A.; Grodecki, K.; Steapniewski, R.; Baranowski, J. M. Transmission electron microscopy and scanning tunneling microscopy investigations of graphene on 4H-SiC(0001). *J. Appl. Phys.* 2009, 105, 023503.
- [34] Jun, S. Density-functional study of edge stress in graphene. *Phys. Rev. B* 2008, 78, 073405.
- [35] Huang, B.; Liu, M.; Su, N.H.; Wu, J.; Duan, W.H.; Gu, B.L.; Liu, F. Quantum manifestations of graphene edge stress and edge instability: A first-principles study. *Phys. Rev. Lett.* 2009, 102, 166404.

- [36] Huang, M.; Yan, H.; Chen, C.; Song, D.; Heinz, T.F.; Hone, J. Phonon softening and crystallographic orientation of strained graphene studied by Raman spectroscopy. *Proc. Natl. Acad. Sci. U.S.A.* 2009, 106, 7304-7308.
- [37] Vozmediano, M.; Katsnelson, M.; Guinea, F. Gauge fields in graphene. *Phys. Rep.* 2010, 496 109-148.
- [38] Novoselov, K.S.; Falko, V.I.; Colombo, L.; Gellert, P.R.; Schwab, M.G.; Kim, K. A roadmap for graphene. *Nature* 2012, 490 192-200.
- [39] Bissett, M.A.; Tsuji, M.; Ago, H. Strain engineering the properties of graphene and other two-dimensional crystals. *Phys. Chem. Chem. Phys.* 2014, 16 11124-11138.
- [40] Roldan, R.; Castellanos-Gomez, A.; Cappelluti, E.; Guinea, F. Strain engineering in semiconducting twodimensional crystals. *J. Phys.: Condens. Matter* 2015, 27 313201.
- [41] Barraza-Lopez, S. Discrete differential geometry and the properties of conformal two-dimensional materials *Synth. Met.* 2015, 210 32-41.
- [42] Galiotis, C.; Frank, O.; Koukaras, E.N.; Sfyris, D. Graphene mechanics: current status and perspectives. *Annu. Rev. Chem. Biomol. Eng.* 2015, 6 121-140.
- [43] Jiang, J.W.; Wang, B.S.; Wang, J.S.; Park, H.S. A review on the flexural mode of graphene: lattice dynamics, thermal conduction, thermal expansion, elasticity and nanomechanical resonance. *J. Phys.: Condens. Matter* 2015, 27 083001.
- [44] Amorim, F.B.; Cortijo, A.; de Juan, F.; Grushin, A.G.; Guinea, F.; Gutiérrez-Rubio, A.; Ochoa, H.; Parente, V.; Roldán, R.; San-Jose, P.; Schiefele, J.; Sturla, M.; Vozmediano, M.A.H. Novel effects of strains in graphene and other two dimensional materials. *Phys. Rep.* 2016, 617 1-54.
- [45] Deng, S.; Berry, V.; Wrinkled, rippled and crumpled graphene: an overview of formation mechanism, electronic properties, and applications. *Mater. Today* 2016, 19 197-212.

- [46] Meunier, V.; Souza Filho, A.G.; Barros, E.B.; Dresselhaus, M.S. Physical properties of low-dimensional sp²-based carbon nanostructures. *Rev. Mod. Phys.* 2016, 88 025005.
- [47] Partoens, B.; Peeters, F.M. From graphene to graphite: Electronic structure around the K point. *Phys. Rev. B* 2006, 74, 075404.
- [48] Yamamoto, T.; Noguchi, T.; Watanabe, K. Edge-state signature in optical absorption of nanographenes: Tight-binding method and time-dependent density functional theory calculations. *Phys. Rev. B* 2006, 74, 121409(R).
- [49] Hsu H., Reichl, L.E. Selection rule for the optical absorption of graphene nanoribbons. *Phys. Rev. B* 2007, 76, 045418.
- [50] Ezawa, M. Metallic graphene nanodisks: Electronic and magnetic properties. *Phys. Rev. B* 2007, 76, 245415.
- [51] Heiskanen, H.P.; Manninen, M.; Akola, J. Electronic structure of triangular, hexagonal and round graphene flakes near the Fermi level. *New J. Phys.* 2008, 10, 103015.
- [52] Yin, H.Q.; Li, W.; Hu, X.; Tao, R.B. Coherent transport of armchair graphene constrictions. *J. Appl. Phys.* 2010, 107, 103706.
- [53] Hancock, Y.; Uppstu, A.; Saloriutta, K.; Harju, A.; Puska, M.J. Generalized tight-binding transport model for graphene nanoribbon-based systems. *Phys. Rev. B* 2010, 81, 245402.
- [54] Zarenia, M.; Chaves, A.; Farias, G.A.; Peeters, F.M. Energy levels of triangular and hexagonal graphene quantum dots: A comparative study between the tight-binding and Dirac equation approach. *Phys. Rev. B* 2011, 84, 245403.
- [55] Hove, L.V. The Occurrence of Singularities in the Elastic Frequency Distribution of a Crystal. *Phys. Rev.* 1953, 89, 1189-1193.
- [56] Hao, L.; Sheng, L. Optical conductivity of multilayer graphene. *Solid State Commun.* 2009, 149, 1962-1966.

- [57] Yang, L.; Deslippe, J.; Park, C.-H.; Cohen, M.L.; Louie, S.G. Excitonic Effects on the Optical Response of Graphene and Bilayer Graphene. *Phys. Rev. Lett.* 2009, 103, 186802.
- [58] Pereira, V.M.; Ribeiro, R.M.; Peres, N.M.R.; Castro Neto, A.H. Optical properties of strained graphene, *EPL* 2010, 92, 67001.
- [59] Born, M.; Wolf, E. *Principles of Optics*, 7th ed. (Pergamon, Oxford, UK, 1999), p. 40.
- [60] Malacara, D. *Optical Shop Testing*, 3rd ed. (John Wiley, USA, 2007), p. 547.
- [61] Falkovsky, L.A.; Pershoguba, S.S.; Optical far-infrared properties of a graphene monolayer and multilayer. *Phys. Rev. B* 2007, 76, 153410.
- [62] Brun, S.J.; Thomsen, M.R.; Electronic and optical properties of graphene and graphene antidot structures. Aalborg University, Aalborg, 2013.
- [63] Pedersen, T.G.; Analytic calculation of the optical properties of graphite. *Phys. Rev. B* 2003, 67, 113106.
- [64] Pellegrino, F.M.D.; Angilella, G.G.N.; Pucci, R. Strain effect on the optical conductivity of graphene. *Phys. Rev. B* 2010, 81, 035411.
- [65] Pedersen, J.G.; Pedersen, T.G. Tight-binding study of the magneto-optical properties of gapped graphene, *Phys. Rev. B* 2011, 84, 035411.